Applied Catalysis B: Environmental 192 (2016) 72–79

Contents lists available at ScienceDirect

Applied Catalysis B: Environmental

journal homepage: www.elsevier.com/locate/apcatb

Visible-light induced photocatalytic oxidative desulfurization using $BiVO_4/C_3N_4@SiO_2$ with air/cumene hydroperoxide under ambient conditions

Guang Miao[a], Dishun Huang[a], Xiaoling Ren[a], Xin Li[b], Zhong Li[a], Jing Xiao[a,*]

[a] Key Laboratory of Enhanced Heat Transfer and Energy Conservation of the Ministry of Education, and School of Chemistry and Chemical Engineering, South China University of Technology, Guangzhou 510640, China
[b] Department of Chemistry, South China University of Agriculture, Guangzhou 510642, China

ARTICLE INFO

Article history:
Received 4 December 2015
Received in revised form 12 March 2016
Accepted 15 March 2016
Available online 16 March 2016

Keywords:
Photocatalytic oxidative desulfurization (PODS)
$BiVO_4/C_3N_4@SiO_2$
Dibenzothiophene
Adsorption
Visible light

ABSTRACT

Trace amount of thiophenic compounds in fuel is harmful to the environment and challenging to get rid of efficiently. The objective of this work is to explore a new visible-light induced photocatalytic oxidative desulfurization (PODS) approach using $BiVO_4/C_3N_4@SiO_2$ with air/cumene hydroperoxide (CHP) under ambient conditions. A series of $BiVO_4/C_3N_4@SiO_2$ photocatalysts were prepared by a hydrothermal method and PODS tests were carried out in a Xenon lamp built-in batch reactor. The dibenzothiophene conversion of the PODS system reached as high as 99%. $BiVO_4/C_3N_4@SiO_2$ showed high vis-photocatalytic activity due to the effective charge separation of $BiVO_4/C_3N_4$ and small particle size of $BiVO_4$. Additional air flow was demonstrated to effectively enhance PODS kinetics of $BiVO_4/C_3N_4@SiO_2$ with CHP, which may be ascribed to the accelerated ROO• generation by air with R• radical for DBT oxidation. Mixing silica gel with $BiVO_4/C_3N_4@SiO_2$ as a hybrid adsorbent under photocatalytic adsorptive desulfurization (PADS) showed a dramatically enhanced desulfurization capacity (7.2 mg/g) compared to that under sole ADS. When fitted to Langmuir adsorption isotherm, K and q_m reached as high as 0.24 and 7.41. The integrated PADS system can be particularly suitable for s single-stage desulfurization for low-sulfur fuel production under visible light at ambient conditions.

1. Introduction

Removal of thiophenic compounds is an important operation in petroleum refining and is achieved by catalytic hydrotreating process operated at elevated temperatures (>300 °C) and high H_2 pressures (20 ~ 100 atm) [1]. The more and more stringent sulfur specification in fuel urged the need of ultra-deep desulfurization, in which hydrotreating becomes more expensive and less efficient as it would require a much larger catalyst bed, higher temperature and pressure, and more H_2 consumption [2]. Therefore, develop alternative non-hydrotreating approaches for effective ultra-deep desulfurization have attracted much recent interests worldwide.

Among various desulfurization technologies, photocatalytic oxidative desulfurization (PODS) received growing attention as it provides a green path to photooxidize sulfur species to highly polar sulfoxide or sulfone products with the utilization of ultraviolet or visible light as the energy source, where photocatalyst plays a key role. TiO_2-based photocatalyst has been widely studied because of its nontoxicity, high chemical and photochemical stability, low cost, and excellent photocatalytic activity under UV irradiation [3]. Zhang et al. [4] prepared TiO_2/bamboo charcoal for the photocatalytic oxidation of dibenzothiophene (DBT) under UV using H_2O_2 as the oxidant, and over 70% of sulfur conversion was reported. Wang et al. [5] synthesized TiO_2/SiO_2 for PODS under UV using air as the oxidant at room temperature, and over 95% of sulfur conversion was reported. However, UV light only accounts for a small fraction (3–5%) of the energy of the sun. Moreover, besides thiophenic compounds, some other fuel components, i.e. aromatics can also absorb UV light strongly [6] and their structure can be destructed during PODS under UV. Therefore, designing photocatalysts responsive to visible light for PODS is desirable.

Bismuth vanadate ($BiVO_4$), with a band gap of 2.4 eV that allows direct photo-activation under visible light [7], is attractive because of its low toxicity, low cost and high stability. However, the photocatalytic activity of $BiVO_4$ under visible light is low in general due to the rapid recombination of photogenerated electrons and holes

* Corresponding author.
E-mail address: cejingxiao@scut.edu.cn (J. Xiao).

http://dx.doi.org/10.1016/j.apcatb.2016.03.033
0926-3373/

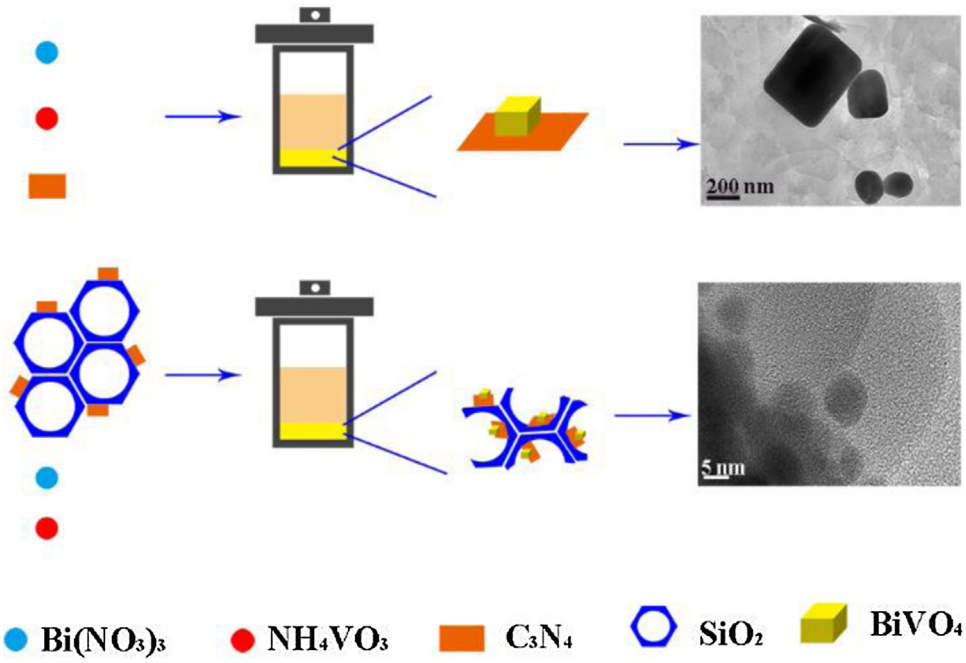

Scheme 1. Schematic illustration of the hydrothermal synthesis of $BiVO_4/C_3N_4$ and $BiVO_4/C_3N_4@SiO_2$.

[8], and thus need to be further enhanced via modification. Lin et al. [6] co-loaded $BiVO_4$ with Pt and RuO_2 as co-catalyst for PODS under visible light using molecular oxygen as the oxidant, which achieved over 99% of thiophene conversion to SO_3. However, using $BiVO_4$-based photocatalyst without the incorporation of precious metal for PODS under visible light has not been addressed in the literature for PODS.

In recent years, carbon nitride (g-C_3N_4) has drawn great attention in photocatalysis due to its visible light absorption, environment stability, and graphene-like 2D structure, etc. [9], which made it applicable as a catalyst or catalyst support in water decomposition, oxygen reduction, organic photosynthesis and environmental remediation [10]. Li et al. [11] synthesized mesoporous TiO_2/g-C_3N_4 hybrid for degradation of methyl orange and phenol, and reported remarkably enhanced photocatalytic activity under visible light. To further enhance the photocatalytic activity, g-C_3N_4 nanosheet was dispersed in mesoporous silica channels, which acted as the support to load Fe^{2+} and Fe^{3+} for the efficient transformation of CO_2 to epoxides and direct oxidative cycloaddition of CO_2 to olefins, respectively [12]. Previous work suggested that g-C_3N_4 dispersed on mesoporous silica can be a new class of effective photocatalyst support, and its visible-light photocatalytic activity may stand out for effective PODS when further hybrid with visible-light responsive $BiVO_4$.

Herein, a new visible-light induced PODS system using g-C_3N_4/SiO_2 supported $BiVO_4$ with air/cumene hydroperoxide (CHP) was investigated and demonstrated to be effective for desulfurization under ambient conditions. The new $BiVO_4/C_3N_4@SiO_2$ photocatalysts were synthesized by hydrothermally loading $BiVO_4$ onto a lab-prepared mesoporous g-C_3N_4/SiO_2 support. The photocatalysts were characterized by N_2 adsorption, X-ray diffraction (XRD) and transmission electron microscope (TEM), Fourier transform infrared spectroscopy (FT-IR) and ultraviolet-visible diffusive reflectance spectroscopy (UV–vis DRS). The effectiveness of $BiVO_4/C_3N_4@SiO_2$ for PODS under visible light was investigated as compared to that of $C_3N_4@SiO_2$, and $BiVO_4@SiO_2$. The synergy between $BiVO_4$ and C_3N_4 on SiO_2 for PODS was further illustrated. The $BiVO_4$ loading and CHP/DBT ratio were optimized. Moreover, the promotion of PODS kinetics by the additional air flow was reported for the first time, and its mechanism was further elucidated. Additionally, the effectiveness of an integrated visible-light induced photocatalytic adsorptive desulfurization (PADS) process by mixing $BiVO_4/C_3N_4@SiO_2$ with silica gel with air/CHP under visible light at ambient conditions was investigated.

2. Experimental

2.1. Photocatalyst syntheses

$BiVO_4/C_3N_4$ and $BiVO_4/C_3N_4@SiO_2$ are synthesized via hydrothermal method. The schematic illustration of the hydrothermal synthesis of $BiVO_4/C_3N_4$ and $BiVO_4/C_3N_4@SiO_2$ were shown in Scheme 1.

The $C_3N_4@SiO_2$ was prepared by a hydrothermal method. In a typical synthesis, 4.0 g P123 was dissolved in 120 ml of water and 20 ml of 12 mol/l HCl solution. Then 9.2 ml of TEOS was added to the above homogeneous solution at 40 °C and mixed for 20 h. After that, 0.5 g melamine as C_3N_4 precursor was added into the slurry, and then the mixture was transferred into a 100 ml Teflon-lined stainless steel autoclave and heated to 110 °C for 24 h. The obtained solids was washed three times with deionized water and dried in a vacuum oven at 80 °C for 8 h. Afterwards, solid product was calcined to 550 °C at a rate of 1.0 °C/min and maintained at 550 °C for 4 h. The powder product was stored in a desiccator for further use.

The $BiVO_4/C_3N_4@SiO_2$ was prepared by loading $BiVO_4$ onto $C_3N_4@SiO_2$ hydrothermally. In a typical synthesis, 0.173 mmol $Bi(NO_3)_3{\cdot}5H_2O$ was dissolved in 0.4 ml of water and 0.2 ml of 14.4 mol/l HNO_3 solution. Then, the solution was added into 0.5 g of as-prepared $C_3N_4@SiO_2$ dropwise under ultrasound for 15 min, and heated at 80 °C for 60 min. Meanwhile, equimolar NH_4VO_3 was dissolved in 50 ml aqueous ammonia and the suspension was heated to dissolve NH_4VO_3. The NH_4VO_3 solution was added into the above solid dropwise, and then the pH of the slurry was adjusted to 7.0 with acetate. This precursor solution was transferred to a Teflon-lined stainless steel autoclave and heated at 180 °C for 16 h at autogenous pressure. After that, the autoclave was cooled to room temperature, and the yellow precipitate was separated by filtration, washed with excess distilled water, and then dried at 100 °C

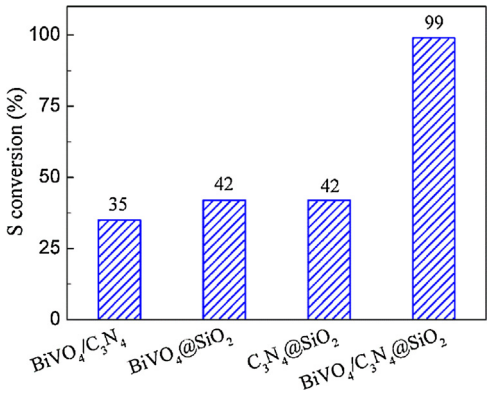

Fig. 1. DBT conversion of $BiVO_4/C_3N_4@SiO_2$ referred to that of $BiVO_4/C_3N_4$, $C_3N_4@SiO_2$ and $BiVO_4@SiO_2$ under PODS at 30 °C (Conditions: initial DBT Conc.: 300 ppm-S; air flow rate: 20 cc/min; fuel-to-catalyst ratio: 20:1; O:S: 3:1).

for 2 h. As a reference, $BiVO_4$ @SiO_2 and $BiVO_4/C_3N_4$ were synthesized by loading $BiVO_4$ onto SiO_2 and C_3N_4, respectively, using the same hydrothermal method mentioned above.

2.2. Characterizations

Nitrogen adsorption isotherms were collected at 77 K using an ASAP2020 analyzer (Micromeritics). The surface area was calculated using BET method. Prior to each measurement, the samples were outgassed at 150 °C for 8 h. Powder X-ray diffraction (XRD) analysis was performed using a Bruker D8 Advance X-ray diffractometer with Cu Kα_1 radiation (λ=1.54056 nm) operated at 40 mA and 40 kV at a scanning range of 10–80° following Joint Committee on Powder Diffraction Standards (JCPDS). Fourier transform infrared spectra (FTIR) of the products were recorded using an IR Affiniy-1 FTIR spectrometer. Transmission electron microscopy (TEM) was conducted using a JEOL2100F. UV–vis diffusive reflectance spectra (UV-vis DRS) were recorded on a Shimadzu UV-2550 UV–vis spectrophotometer using $BaSO_4$ as the reference.

Atomic Absorption Spectroscopy (AAS) was used to quantify the Bi content in the composites.

2.3. Model fuel (MDF)

The model fuels were prepared by dissolving given amounts (100–400 ppmw) of dibenzothiophene (DBT, 98%) in dodecane (99%). All the chemicals were purchased from Sigma–Aldrich and used as such without further purification.

2.4. Photocatalytic oxidative desulfurization (PODS) test

Schematic illustration of the PODS reactor with a built-in Xenon lamp was shown in **Fig. S1.** The photocatalyst was mixed with model fuel (certain amount of CHP was added) in a given ratio in the PODS reactor. The water cooled condenser was installed above the reactor to avoid the liquid loss (~3%). The treated fuels were sampled periodically. Air flow rate for PODS was set as 20 cc/min. The DBT concentration in initial and desulfurized fuels were monitored by a high-performance liquid chromatogram (HPLC) equipped with a UV–vis detector at 301 nm and an ODS-C18 column at the flow rate of 1.0 cc/min. The oxidation product of DBT in treated fuel was identified by GC–MS. The program was initially set at 50 °C and ramped immediately at 10 °C/min to 100 °C, followed by a ramp at 25 °C/min to 280 °C, and held at 280 °C for 5 min.

2.5. Adsorption isotherms of $BiVO_4/C_3N_4@SiO_2$ mixed with silica gel

The effectiveness of the integrated visible-light induced PADS process was tested by the adsorption isotherms of mixed $BiVO_4/C_3N_4@SiO_2$ with silica gel. The adsorption isotherms of $BiVO_4/C_3N_4@SiO_2$ mixed with silica gel (weight ratio of 4:1) under PADS and sole ADS were carried out in a stirred batch system. About 4.0 g of model fuel (100, 200, 300, 400 ppmw-S of DBT in dodecane) and 0.2 g of $BiVO_4/C_3N_4@SiO_2$ mixed with 0.05 g of silica gel (Sigma–Aldrich, S_{BET} of 330m^2/g) were mixed under ambient conditions till reached adsorption equilibrium (2 h) unless mentioned otherwise. The treated fuels were sampled and tested using a HPLC equipped with a UV–vis detector at 301 nm.

3. Results and discussion

3.1. Effectiveness of $BiVO_4/C_3N_4@SiO_2$ for PODS

Fig. 1 shows DBT conversion of $BiVO_4/C_3N_4@SiO_2$ and its three references. The DBT conversion reached as high as 99%, demonstrating that $BiVO_4/C_3N_4@SiO_2$ acted as an effective photocatalyst for deep desulfurization of fuels under visible light at ambient conditions. Moreover, compared to $C_3N_4@SiO_2$ and $BiVO_4@SiO_2$, a 2.4-times higher DBT conversion was achieved by $BiVO_4/C_3N_4@SiO_2$, suggesting the synergy between $BiVO_4$ and C_3N_4 was present on the photocatalytic conversion of DBT. Meanwhile, compared to $BiVO_4/C_3N_4$ without SiO_2 support, a tripled DBT conversion was achieved on $BiVO_4/C_3N_4@SiO_2$, which suggested that SiO_2 in $BiVO_4/C_3N_4@SiO_2$ played a critical role for the effective photocatalytic oxidation of DBT. Fig. S**2** shows the effect of $BiVO_4$ loading in $BiVO_4/C_3N_4@SiO_2$ on DBT conversion. The $BiVO_4$ loading was optimized to be 8.6%.

Table 1 lists BET surface area (S_{BET}) of $BiVO_4/C_3N_4@SiO_2$ referred to that of $BiVO_4/C_3N_4$, $BiVO_4@SiO_2$, $C_3N_4@SiO_2$ and the parent SiO_2. It was noted that with the incorporation of C_3N_4 into SiO_2 hydrothermally, its S_{BET} increased slightly from 920.4 to 933.4 m^2/g, which may be ascribed to the newly generated porosity by anchoring C_3N_4 into SiO_2. By further incorporation of $BiVO_4$ into $C_3N_4@SiO_2$, a dramatic decrease of S_{BET} (from >900 to only 8.0 m^2/g) was noticed. Similarly, $BiVO_4/C_3N_4@SiO_2$ at 4.4, 8.6, and 13.2% of $BiVO_4$ loading were measured to be ~0 m^2/g. $BiVO_4@SiO_2$ also had a much lower S_{BET} (42.7 m^2/g) than the parent SiO_2. Fig. S**6** showed the TEM images of the $BiVO_4@SiO_2$ sample after hydrothermal process. The results suggested that pores in $C_3N_4@SiO_2$ or SiO_2 collapsed in the process of $BiVO_4$ incorporation into $C_3N_4@SiO_2$ or SiO_2, due likely to the high hydrothermal temperature [13] during the synthesis of $BiVO_4@SiO_2$ and $BiVO_4/C_3N_4@SiO_2$. It should be mentioned that though $BiVO_4/C_3N_4@SiO_2$ had lower S_{BET} than $BiVO_4@SiO_2$ and $C_3N_4@SiO_2$, it showed the highest DBT conversion (Fig. 1), suggesting the synergy between $BiVO_4$ and C_3N_4 was not dominated by the textural properties.

Fig. 2 shows the XRD pattern of $BiVO_4/C_3N_4@SiO_2$ photocatalyst referred to that of $BiVO_4/C_3N_4$, $C_3N_4@SiO_2$ and $BiVO_4@SiO_2$.

Table 1
BET surface area of $BiVO_4/C_3N_4@SiO_2$ referred to that of $BiVO_4/C_3N_4$, $BiVO_4@SiO_2$, $C_3N_4@SiO_2$ and the parent SiO_2.

Sample	$BiVO_4/C_3N_4@SiO_2$	$BiVO_4/C_3N_4$	$BiVO_4@SiO_2$	$C_3N_4@SiO_2$	SiO_2
S_{BET} (m^2/g)	8.0	<5.0[a]	42.7	933.4	920.4

[a] Under the detection limit of ASAP2020.

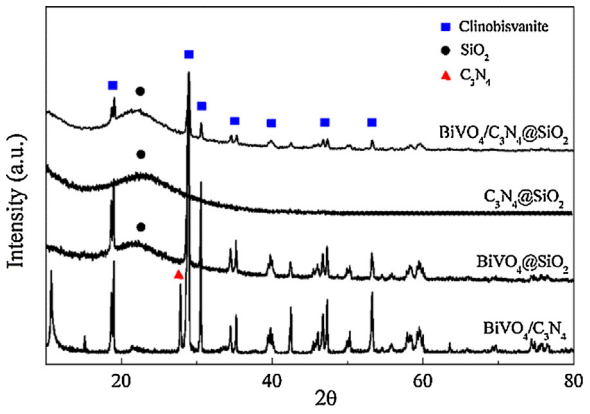

Fig. 2. XRD patterns of $BiVO_4/C_3N_4@SiO_2$ photocatalyst referred to that of $BiVO_4/C_3N_4$, $C_3N_4@SiO_2$ and $BiVO_4@SiO_2$.

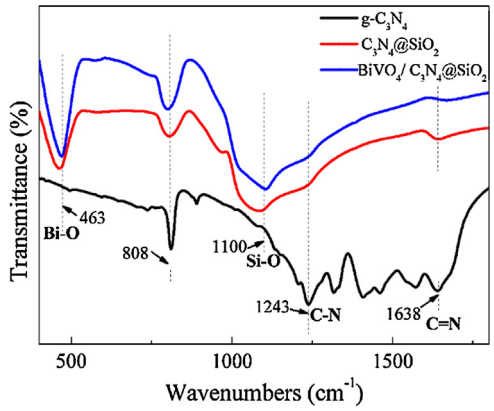

Fig. 3. FI-IR spectra of $BiVO_4/C_3N_4@SiO_2$ photocatalyst referred to that of $C_3N_4@SiO_2$ and g-C_3N_4.

For $BiVO_4/C_3N_4@SiO_2$, $BiVO_4@SiO_2$, and $BiVO_4/C_3N_4$ samples, the diffraction peaks at 2θ of 18.6°, 28.8°, 34.5°, 39.8°, 42.7°, 46.1°, 47.3°, and 53.4° were clearly observed, which correspond to the crystalline planes of (101), (112), (200), (211), (015), (220), (123) and (116), respectively, characteristics of monoclinic $BiVO_4$[7]. Compared to $BiVO_4/C_3N_4$, $BiVO_4/C_3N_4@SiO_2$ showed a weakened featured peaks of monoclinic $BiVO_4$, suggesting the crystallinity of monoclinic $BiVO_4$ decreased after incorporated into SiO_2. It should be mentioned that the characteristic peak (~27.4° [14]) for C_3N_4 was identified for $BiVO_4/C_3N_4$ (90%), but not for $C_3N_4@SiO_2$ and $BiVO_4/C_3N_4@SiO_2$ in Fig. 2, similar to that of g-C_3N_4/NiFe-LDH composite [15], GO/MIL-101 [16] and Ag_3VO_4/C_3N_4 hybrid materials [17]. This was possibly due to the low C_3N_4 loading (0.46 wt.%) in the composites. Scherrer equation $D = (K \times \lambda)/(\beta \times \cos\theta)$. ($K = 0.89$, $\lambda = 1.54$ nm) was applied to calculate the average particle sizes of $BiVO_4$ in the $BiVO_4/C_3N_4@SiO_2$ sample, which was in the range of 3–8 nm, and $BiVO_4$ (112) plane was dominating. Fig. 3 presents the FI-IR spectra of $BiVO_4/C_3N_4@SiO_2$ photocatalyst referred to that of $C_3N_4@SiO_2$ and g-C_3N_4. The breathing vibration at 808 cm^{-1} for triazine units, the skeletal vibration bands at 1243 cm^{-1} and 1638 cm^{-1} for aromatic C—N and C=N heterocycles, characteristic bands for g- C_3N [9a,18], were commonly present for all the three samples, suggesting the successful incorporation of C_3N_4 in $C_3N_4@SiO_2$ as well as $BiVO_4/C_3N_4@SiO_2$.

Fig. 4 shows the TEM images of $BiVO_4/C_3N_4@SiO_2$ sample referred to that of $BiVO_4/C_3N_4$, $C_3N_4@SiO_2$ and $BiVO_4@SiO_2$. The $BiVO_4$ facet spacing of 0.309 nm in Fig. 4a,c and d, characteristic of (112) crystalline plane for monoclinic $BiVO_4$, suggested that the monoclinic $BiVO_4$ was the dominated crystalline structure in both $BiVO_4@SiO_2$ and $BiVO_4/C_3N_4@SiO_2$, which was consistent with the XRD results in Fig. 2. For $BiVO_4/C_3N_4$ (Fig. 4a), the particle size of monoclinic $BiVO_4$ (located above C_3N_4) was in hundreds of nm. In sharp contrast, $BiVO_4@SiO_2$ and $BiVO_4/C_3N_4@SiO_2$ had much smaller particle sizes of monoclinic $BiVO_4$ (averagely 5–6 nm), which was in accordance with the average particle size calculated by Scherrer equation from Fig. 2. The result suggested that the particle size of $BiVO_4$ decreased dramatically after the hydrothermal incorporation of $BiVO_4$. It was likely that $BiVO_4$ was initially dispersed well on the highly porous $C_3N_4@SiO_2$ or SiO_2 support (S_{BET} over 900 m^2/g in Table 1) forming small particles of $BiVO_4$, and the particles did not aggregate to much larger particles during the later corrosion (pore collapses, Fig. 4c) stage of $C_3N_4@SiO_2$ or SiO_2 when introducing $BiVO_4$ hydrothermally. The particle size of $BiVO_4$ was noted to follow the order of $BiVO_4@SiO_2 \sim BiVO_4/C_3N_4@SiO_2 < BiVO_4/C_3N_4$. However, $BiVO_4@SiO_2$ showed lower DBT conversion than $BiVO_4/C_3N_4@SiO_2$ (Fig. 1), suggesting the particle size of $BiVO_4$ alone was not the dominating factor for the photocatalytic DBT conversion. Moreover, it was noted in Fig. 4d that different from $BiVO_4@SiO_2$, $BiVO_4$ located above C_3N_4 rather than SiO_2 in $BiVO_4/C_3N_4@SiO_2$ (achieved 99% of DBT conversion in Fig. 1). The results indicated that the anchoring of $BiVO_4$ on C_3N_4 may play a critical role on PODS.

Fig. 5 shows the UV–vis DRS of $BiVO_4/C_3N_4@SiO_2$ referred to that of $BiVO_4@SiO_2$ and $C_3N_4@SiO_2$. $C_3N_4@SiO_2$ shows an absorption region at 300–500 nm (a portion in the visible light region) and reaches the highest adsorption at 340 nm, consistent with those reported in the literature [9a,19]. The absorption strength was quite low, which can be attributed to the low content of C_3N_4 (0.46 wt.%) in the $C_3N_4@SiO_2$ sample. $BiVO_4@SiO_2$ shows an absorption range at 300–550 nm and reaches the highest adsorption at 480 nm, clearly visible light-sensitive [7,20]. Interesting, by incorporating $BiVO_4$ into $C_3N_4@SiO_2$, it gives a broad peak region at 300–550 nm, and its absorption intensity was much stronger than that of $BiVO_4@SiO_2$ and $C_3N_4@SiO_2$. The results indicated that the synergy between C_3N_4 and $BiVO_4$ on visible light absorption was present, which was further illustrated in the inset of Fig. 5. At the interface of the composites, the hybridization of $BiVO_4$ and C_3N_4 reduce the electron density in the VB of $BiVO_4$ and the CB of C_3N_4, which was beneficial for the VB electrons into the CB of C_3N_4 and thus promoted the transformation of CB electrons to the surface of $BiVO_4$. Meanwhile, the electron mobility was improved due to the delocalized conjugated structure of C_3N_4, which reduced the possibility of hole-electron recombination. On one hand, different position of energy band between C_3N_4 and $BiVO_4$ contributed to the formation of heterojunction, which increased the adsorption intensity at visible light region. On the other hand, the photoinduced electrons and holes participated in PODS and transformed CHP into $OH^•$ and $ROO^•$, which further served as the oxidant for DBT. Therefore, the effective charge separation decreased the probability of hole-electron recombination and resulted in the enhanced photocatalytic activity under visible light irradiation [21]. It should be mentioned that the synergy between C_3N_4 and $BiVO_4$ can be also present in the $BiVO_4/C_3N_4$ sample. However, its larger particle size of $BiVO_4$ (hundreds of nm, Fig. 4) may negatively impact its catalytic activity for DBT conversion (35%). In other word, smaller particle size of $BiVO_4$ in $BiVO_4/C_3N_4$ hybrid may impact its photocatalytic activity for DBT conversion. To sum up, the high DBT conversion of $BiVO_4/C_3N_4@SiO_2$ may be attributed to the anchoring $BiVO_4$ onto C_3N_4 for enhanced charge separation and the small particle size (nano-scale, Fig. 4) of $BiVO_4$ for superior photocatalytic activity. Additionally, the highest DBT conversion of 8.6% $BiVO_4/C_3N_4@SiO_2$ may be ascribed to the balanced $BiVO_4$ —C_3N_4 charge transfer effect and particle size effect at the $BiVO_4$ loading of 8.6%.

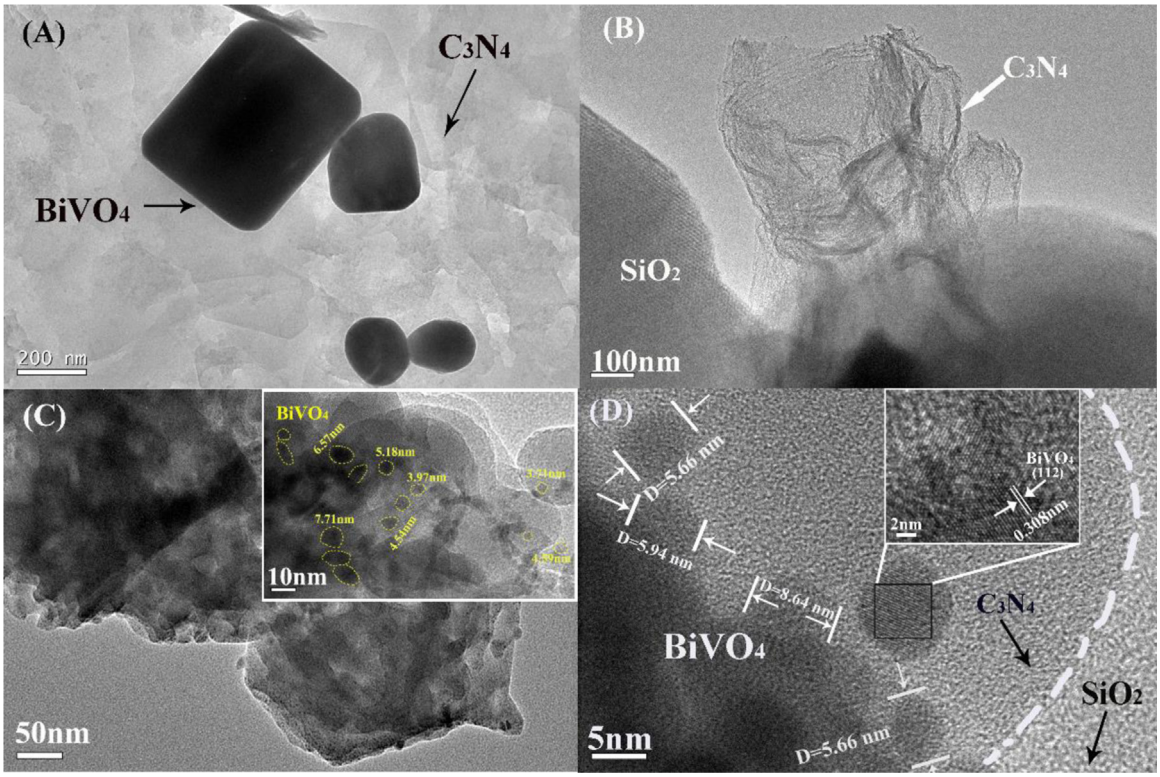

Fig. 4. TEM images of (A) $BiVO_4/C_3N_4$; (B) $C_3N_4@SiO_2$; (C) $BiVO_4@SiO_2$; (D) $BiVO_4/C_3N_4@SiO_2$.

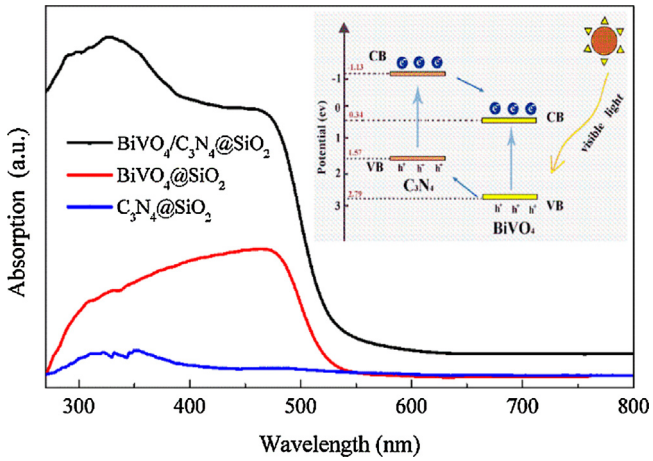

Fig. 5. UV–vis DRS of $BiVO_4/C_3N_4@SiO_2$ referred to $BiVO_4@SiO_2$ and $C_3N_4@SiO_2$ (Inset: Schematic illustration of effective charge separation of hybrid C_3N_4 and $BiVO_4$ under visible light).

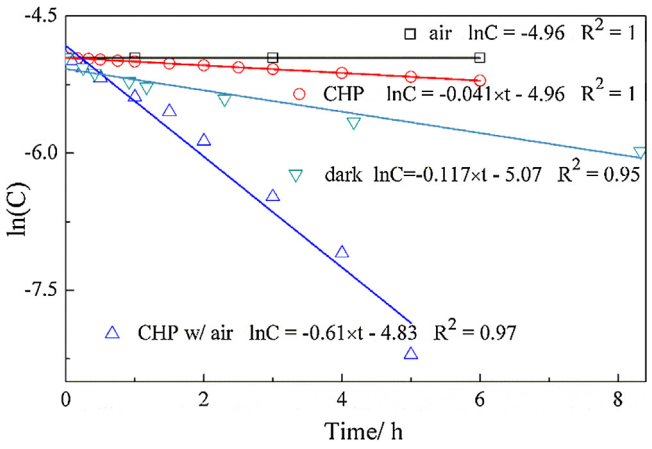

Fig. 6. Plots of ln C_t versus time during PODS.

3.2. *Effects of air and CHP on PODS*

Molecular oxygen is an ideal "green" oxidant for the oxidation of thiophenes. However, due to its triplet ground state structure, molecule oxygen is an inactive molecule for thiophene oxidation. Cumene hydroperoxide (CHP) is a more active oxidant due to its oxidation state of −1 for oxygen, and thus was selected as the suitable oxidant for oxidative desulfurization [22]. In this work, applying air and CHP together as compared to that separately for PODS was investigated. Fig. S3 shows the effect of air flow on PODS kinetics of DBT over $BiVO_4/C_3N_4@SiO_2$ using CHP. Interestingly, though only 20% of DBT conversion was achieved by $BiVO_4/C_3N_4@SiO_2$ using CHP in 5 h, it was dramatically enhanced when air flow was introduced simultaneously, the DBT conversion reached 99% in 5 h. It should be mentioned that under dark condition, $BiVO_4/C_3N_4@SiO_2$ showed moderate catalytic activity for BDT oxidation in the presence of both oxygen and CHP. And with the involvement of visible light, the rate constant was greatly enhanced (5.2 times higher), suggesting the presence of light accelerated the DBT oxidation process vastly. The results suggested that PODS using $BiVO_4/C_3N_4@SiO_2$ by applying air and CHP simultaneously was able to deeply desulfurize DBT under visible light at ambient conditions.

The kinetic curves of PODS over $BiVO_4/C_3N_4@SiO_2$ using different oxidants were further fitted to the first order reaction equation: $-\frac{dC(t)}{dt} = kC(t)$, where k is the rate constant and C(t) is the concentration of sulfur compounds in the liquid phase varied with time, and then converted to the fitting plots of $ln(C)$ versus t, as shown in Fig. 6. Good linear relationships were obtained between $ln(C)$ and t (correlation coefficients $R^2 \geq 95\%$), indicating that the PODS kinetics can be well expressed by the

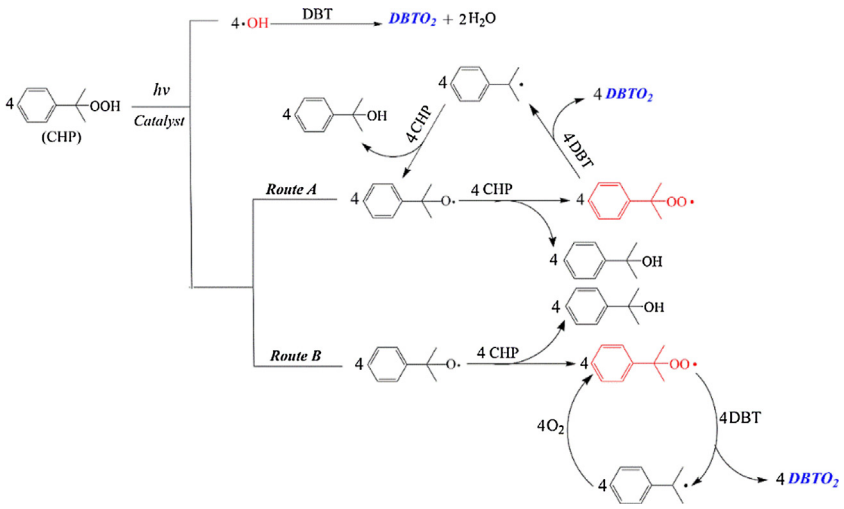

Fig. 7. Possible PODS pathway using CHP w/o and w/O_2.

first-order kinetic models. The rate constant increased in the order of air < CHP < dark < air + CHP (0, 0.041, 0.117 and 0.61 h^{-1} respectively), suggesting the reaction activation energy increased in the order of air + CHP < dark < CHP < air. The results implied that the introduction of air flow and light accelerated DBT conversion on $BiVO_4/C_3N_4@SiO_2$ with CHP, which may be ascribed to the O_2 —CHP synergistic mechanism under visible light on DBT oxidation as further studied in the 3.3 Section.

Fig. S**4** shows the effect of CHP/DBT ratio on the DBT conversion. The DBT conversion followed the order of 3:1 > 4:1 > 8:1 > 2:1. The optimized CHP/DBT ratio of 3:1 was higher than the stoichiometric ratio of 2 molar of CHP reacted with 1 molar of DBT forming $DBTO_2$ [23], which may be ascribed to the partial self-photodegradation of CHP to alcohol [24]. It should be noted that if further increase O/S ratio from 3:1 to 4:1 or 8:1, the PODS capacity decreased. The results may be ascribed to the oxidation of small portion of dodecane (the MDF solvent) when CHP was in excess. The as-formed polar byproducts, i.e. alcohol [25] occupied the PODS catalytic sites on $BiVO_4/C_3N_4@SiO_2$, and thus resulted in decreased DBT conversion at increased O/S ratio.

3.3. Pathways of PODS

To understand the PODS mechanism using air and CHP simultaneously, radial scavengers [26], isopropanol (capture ROO• radical), benzoquinone (capture HO• radical) and methanol (capture hole) were introduced to detect and quantify the intermediate radials for PODS. Table 2 lists DBT conversion of $BiVO_4/C_3N_4@SiO_2$ under different radial scavengers. 71.8, 27.2, and 99.0% of DBT conversion were achieved when isopropanol, benzoquinone and methanol were introduced during PODS. The results suggested that two types of radicals (71.8% of ROO• and 27.2% of HO•) rather than the hole served as the intermediate oxidants for PODS, and ROO• was more significant. With that, the possible PODS pathway using CHP w/o and w/air were proposed in Fig. 7. The PODS was initiated with the generation of HO• and RO• from CHP [23] under visible light irradiation. Followed with that, RO• was further oxidized to ROO• radical by CHP [27]. After that, the ROO• and HO• radicals served as the intermediate for DBT oxidation to $DBTO_2$ [27], where the ROO• itself was reduced to R•. Without the additional O_2, R• was further oxidized to RO•, and then ROO• by CHP (**Route A**), which further served as the intermediate for DBT oxidation to $DBTO_2$. In contrast, with the additional O_2, R• reacted with O_2 molecule to generate ROO• directly [27] for DBT oxidation without the step of intermediate RO• formation by CHP (**Route B**), as the Gibbs free energy of CHP-R• reaction (−18.2 kcal/mol) was higher than that of O_2-R• reaction (−19.2 kcal/mol) [27], and thus promoted the PODS kinetics. The proposed PODS pathways explained the dramatically enhanced PODS from kinetics and thermodynamics when air was introduced (Fig. S**3**) through **Route B**.

Table 2
DBT conversion of $BiVO_4/C_3N_4@SiO_2$ under visible light using three radial scavengers.

Scavengers	N/A	isopropanol	benzoquinone	methanol
DBT conversion/%	99.0	71.8	27.2	99.0

Fig. S**5** shows the GC–MS pattern of sulfur species in the treated fuel. It was confirmed that dibenzothiophene sulfone ($DBTO_2$) was identified as the PODS product when applying $BiVO_4/C_3N_4@SiO_2$ as the photocatalyst using air and CHP simultaneously under visible light, which is the same as the PODS product identified in CHP/TiCeO-MCM-48 [28], H_2O_2/WOx-ZrO_2 [29], and CHP/Al_2O_3—CuO [23] systems, but different from the oxidation product of dibenzothiophene sulfoxide (DBTO) in UV-photocatalytic ADS over TiO_2/SiO_2 [30]. During the oxidation process, it was noted that part of the oxidation product $DBTO_2$ was not desorbed from the $BiVO_4/C_3N_4@SiO_2$ surface. It was likely that SiO_2 acted as the adsorbent for $DBTO_2$ through the abundant surface silanol groups.

3.4. Regeneration of $BiVO_4/C_3N_4@SiO_2$

Fig. 8 shows the DBT conversion of the $BiVO_4/C_3N_4@SiO_2$ in 4 consecutive regeneration cycles. It can be seen that the $BiVO_4/C_3N_4@SiO_2$ photocatalyst can be well regenerated by solvent wash followed with calcination under air. It was also noted that the desulfurization capacities slightly decreased with regeneration cycles, which can be ascribed to the loss of active component $BiVO_4$ during the PODS process, similar phenomenon was reported by Hauser et al. [31].

3.5. Effectiveness of the integrated PADS process

The thiophenic compounds was oxidized to thiophenic sulfones during PODS, which were required to be further removed in a followed-up process, such as adsorption by polar adsorbents or extraction by polar extractants, i.e. water, acetonitrile, or ionic liquids (ILs) [32], to completely subtract sulfur element from fuel. Herein, an integrated photocatalytic adsorptive desulfurization (PADS) process, PODS combined with sulfone adsorption

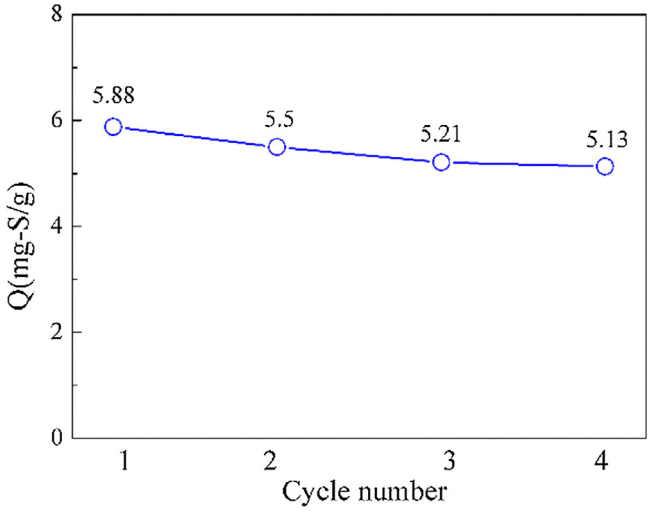

Fig. 8. DBT conversion of the $BiVO_4/C_3N_4@SiO_2$ at 4 consecutive regeneration (Regeneration conditions:Catalyst was washed by 10 ml ethanol and 10 ml acetone for 3 times and then calcined at 300 °C for 4 h).

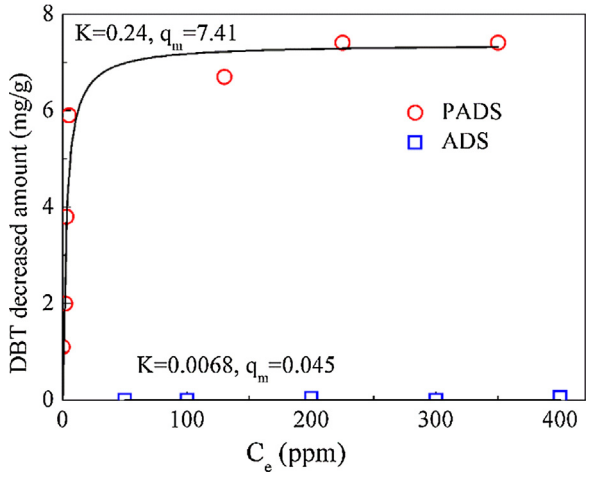

Fig. 9. Adsorption isotherms of DBT over $BiVO_4/C_3N_4@SiO_2$ mixed with silica gel under PADS referred to that under sole adsorption.

using mixed $BiVO_4/C_3N_4@SiO_2$ photocatalyst with silica gel under air/CHP under ambient conditions was investigated. To verify the effectiveness of the PADS process, the adsorption isotherms of mixed $BiVO_4/C_3N_4@SiO_2$ photocatalyst with silica gel under PADS referred to that under sole ADS were compared as shown in Fig. 9. In sharp contrast, $BiVO_4/C_3N_4@SiO_2$ mixed with silica gel under PADS process showed a significantly higher desulfurization capacity compared to that under sole ADS. Particularly, at the low C_e of 15 and 5 ppm-S, desulfurization capacity of $BiVO_4/C_3N_4@SiO_2$ mixed with silica gel reached as high as 5.0 and 4.0 mg-S/g-sorb under PADS, while negligible desulfurization capacity was obtained on that under sole ADS.

The static adsorption data were further fitted to the Langmuir adsorption isotherm model $Q = q_m{}^*k^*C_e/(1 + k^*C_e)$, where Q is the equilibrium amount adsorbed of sulfur on the $BiVO_4/C_3N_4@SiO_2$ mixed with silica gel, C_e is the concentration of DBT in the liquid phase at equilibrium, k is the adsorption equilibrium constant, and q_m is the maximum adsorption capacity of DBT. The much greater k of 0.24 under PADS suggested that the adsorption affinity was dramatically enhanced after the transformation of DBT to $DBTO_2$, which may be ascribed to the strong adsorption affinity of silica gel to the highly polar $DBTO_2$ rather than DBT [23]. The isotherm results further suggested that applying the integrated PADS process by mixing $BiVO_4/C_3N_4@SiO_2$ with silica gel under visible light was effective for fuel desulfurization at low sulfur concentration range. It should be highlighted that the desulfurization capacity of the integrated PADS system was higher than the previously reported UV photocatalytic ADS-TiO_2/SiO_2 system [5], as well as many reported desulfurization adsorbents at low S-concentration range (<15 ppm-S), such as carbon materials [33], UMCM-150 and HKUST [34], etc., which made it promising to be engineered for the effective deep desulfurization of fuel.

4. Conclusion

In this work, an effective PODS approach using $BiVO_4/C_3N_4@SiO_2$ with air/CHP under ambient conditions was developed. The following conclusions can be drawn:

(a) The DBT conversion of $BiVO_4/C_3N_4@SiO_2$ under PODS reached as high as 99%, which was much higher than that of $BiVO_4/C_3N_4$, $BiVO_4@SiO_2$ and $C_3N_4@SiO_2$. The highest vis-photocatalytic activity of $BiVO_4/C_3N_4@SiO_2$ could be ascribed to the effective charge separation formation of $BiVO_4/C_3N_4$ and small particle size of $BiVO_4$.
(b) The additional air flow dramatically enhanced the PODS kinetics of $BiVO_4/C_3N_4@SiO_2$ with CHP, which may be ascribed to the accelerated ROO• radical formation by the introduced O_2 with R• radical for the DBT oxidation.
(c) The $BiVO_4$ loading and the CHP/DBT ratio were optimized to be 8.6% and 3:1.
(d) Mixing $BiVO_4/C_3N_4@SiO_2$ with silica gel as a hybrid adsorbent under PADS showed a dramatically enhanced desulfurization capacity (7.2 mg/g) compared to that under pure ADS, with a high K of 0.24 and q_m of 7.41 were obtained when fitted to Langmuir adsorption isotherm. The integrated PADS approach further simplified the desulfurization process and can pave the way for a single stage desulfurization process using air/CHP for producing low sulfur fuels.

Acknowledgements

We gratefully acknowledge the research grants provided by the National Natural Science Foundation of China (21306054), Guangdong Natural Science Foundation (S2013040014747, 2014A030312007), Guangdong Natural Science Funds for Distinguished Young Scholar, Petro China Innovation Foundation, the Scientific Research Foundation for the Returned Overseas Chinese Scholars, State Education Ministry, and Fundamental Research Funds for the Central Universities.

Appendix A. Supplementary data

Supplementary data associated with this article can be found, in the online version, at http://dx.doi.org/10.1016/j.apcatb.2016.03.033.

References

[1] (a) R.T. Yang, Y.H. Wang, J.M. Heinzel, Ind. Eng. Chem. Res. 48 (2009) 142–147; (b) C.S. Song, X.L. Ma, Appl. Catal. B Environ. 41 (2003) 207–238.
[2] X.L. Ma, S. Velu, J.H. Kim, C.S. Song, Appl. Catal. B Environ. 56 (2005) 137–147.
[3] (a) C. Su, X. Ran, J. Hu, C. Shao, Environ. Sci. Technol. 47 (2013) 11562–11568; (b) X. Guo, D. M, J. Crittenden, Environ. Sci. Tech. 49 (2015) 9230–9236.
[4] J. Zhang, D.S. Zhao, J. Wang, L. Yang, J. Mater. Sci. 44 (2009) 3112–3117.
[5] X. Wang, W. Zhang, L. Wu, F. Ye, J. Xiao, Z. Li, RSC Adv. 4 (2014) 56567–56570.
[6] F. Lin, D.G. Wang, Z.X. Jiang, Y. Ma, J. Li, R.G. Li, C. Li, Energ. Environ. Sci. 5 (2012) 6400–6406.
[7] J. Tang, B. Song, Q. Deng, H. Xin, Mater. Sci. Semicond. Process 35 (2015) 90–95.

[8] (a) J.W. Yang, D.H. Han, C. Li, Acc. Chem. Res. 46 (2013) 1900–1909;
(b) J. Cheng, J.W. Pan, ACS Appl. Mater. Interfaces 7 (2015) 9638–9644.
[9] (a) M. Ding, W. Wang, Y. Zhou, C. Lu, Y. Ni, Z. Xu, J. Alloys Compd. 635 (2015) 34–40;
(b) W.Y. Wang, C. J, D. Xia, P.K. Wong, Y. Li, Environ. Sci. Tech. 47 (2013) 8724–8732.
[10] P. Zhang, Y. Wang, H. Li, M. Antonietti, Green Chem. 14 (2012) 1904–1908.
[11] Y. Li, J. Wang, Y. Yang, Y. Zhang, D. He, Q. An, G. Cao, J. Hazard. Mater. 292 (2015) 79–89.
[12] Z. Huang, F. Li, B. Chen, T. Lu, Y. Yuan, G. Yuan, Appl. Catal. B Environ. 136–137 (2013) 269–277.
[13] D.Y. Zhao, J.L. Feng, Q.S. Huo, N. Melosh, G.H. Fredrickson, B.F. Chmelka, G.D. Stucky, Science 279 (1998) 548–552.
[14] M. Zhang, X. Bai, D. Liu, J. Wang, Y. Zhu, Appl. Catal. B Environ. 164 (2015) 77–81.
[15] S.M. Nayak, L.K. Parida, J. Mater. Chem. A 3 (2015) 18622–18635.
[16] J. Yan, Y. Yu, C. Ma, J. Xiao, Q. Xia, Y. Li, Z. Li, Appl. Therm. Eng. 84 (2015) 118–125.
[17] S. Wang, D. Li, C. Sun, S. Yang, Y. Guan, H. He, Appl. Catal. B Environ. 144 (2014) 885–892.
[18] (a) D. Chen, K. Wang, W. Hong, R. Zong, W. Yao, Y. Zhu, Appl. Catal. B Environ. 166 (2015) 366–373;
(b) J. Zhang, M. Z, C. Yang, X. Wang, Adv. Mater. 26 (2014) 4121–4126;
(c) S. Wu, K. L, W. Zhang, Appl. Surf. Sci. 324 (2015) 324–331.
[19] H. Zhao, C. Di, L. Wang, Y. Chun, Q. Xu, Micropor. Mesopor. Mat. 208 (2015) 98–104.
[20] M.J. Nalbandian, M. Zang, J. Sanchez, Y. Choa, D.M. Cwiertny, N.V. Myung, J. Mol. Catal. a-Chem. 404 (2015) 18–26.
[21] (a) S. Chen, Y. Qi, T. Hisatomi, Q. Ding, T. Asai, Z. Li, S. Ma, K. S, F. Zhang, K. Domen, C. Li, Angew. Chem. Int. Ed. 54 (2015) 1–5;
(b) Z. Chen, F. Bing, Q. Liu, Z. Zhang, X. Fang, J. Mater. Chem. A 3 (2015) 4652–4658.
[22] (a) G.W. Mushrush, E.J. Beal, D.R. Hardy, R.N. Hazlett, D.G. Mose, Fuel 73 (1994) 1481–1485;
(b) J. Xiao, L. W, Y. Wu, B. Liu, L. Dai, Z. Li, Q. Xia, H. Xi, Appl. Energy 113 (2014) 78–85.
[23] C.S. Song, R. Sundararaman, X.L. Ma, Ind. Eng. Chem. Res. 49 (2010) 5561–5568.
[24] W. Zhang, J. Xiao, X. Wang, G. Miao, F. Ye, Z. Li, EnergyFuels 28 (2014) 5339–5344.
[25] (a) R.G. Lichtenthaler, W.R. Haag, T. Mill, Environ. Sci. Technol. 23 (1989) 39–45;
(b) J.R. Payne, C.R. Phillips, Environ. Sci. Technol. 19 (1985) 569–579.
[26] J.H. Kou, Z. Li, Y. Yuan, H. Zhang, Y. Wang, Z. Zou, Environ. Sci. Technol. 43 (2009) 2919–2924.
[27] S. Matsui, T. Fujita, Catal. Today 71 (2001) 145–152.
[28] J. Xiao, X.X. Wang, Y.S. Chen, M. Fujii, C.S. Song, Ind. Eng. Chem. Res. 52 (2013) 15746–15755.
[29] E. Torres-Garcia, A. Galano, G. Rodriguez-Gattorno, J. Catal. 282 (2011) 201–208.
[30] G. Miao, F. Ze, L. Wu, X. Ren, J. Xiao, Z. Li, H.H. Wang, J. Hazard. Mater. (2015).
[31] J.L. Hauser, D.T. Tran, E.T. Conley, Chem. Mater. 28 (2015) 474–479.
[32] F. Li, Y. Liu, Z. Sun, Y. Zhao, R. Liu, L. Chen, D. Zhao, Catal. Sci. Technol. 2 (2012) 1455–1462.
[33] (a) M.X. Yu, Z. Li, Q.B. Xia, S.W. Wang, J. Chem. Ind. Eng. (China) 58 (2007) 938–943;
(b) A.N. Zhou, X.L. Ma, C.S. Song, J. Phys. Chem. B 110 (2006) 4699–4707;
(c) L. Wu, S. S, J. Xiao, B. Liu, Z. Li, M.J. Janik, Chem. Eng. J. 242 (2014) 211–219.
[34] (a) A.J. Matzger, K.A. Cychosz, A.G. Wong-Foy, J. Am. Chem. Soc. 131 (2009) 14538–14543;
(b) L. Wu, J. X, Y. Wu, S. Xian, G. Miao, H.H. Wang, Z. Li, Langmuir 30 (2014) 1080–1088.